

A 3D Fractal-Based Approach towards Understanding Changes in the Infarcted Heart Microvasculature*

Polyxeni Gkontra¹, Magdalena M. Żak¹, Kerri-Ann Norton²,
Andrés Santos³, Aleksander S. Popel², and Alicia G. Arroyo¹

¹ Centro Nacional de Investigaciones Cardiovasculares Carlos III (CNIC),
Madrid, Spain

² Department of Biomedical Engineering, School of Medicine,
Johns Hopkins University, Baltimore, MD, US

³ Universidad Politécnica de Madrid and CIBERBBN, Spain

Abstract. The structure and function of the myocardial microvasculature affect cardiac performance. Quantitative assessment of microvascular changes is therefore crucial to understanding heart disease. This paper proposes the use of 3D fractal-based measures to obtain quantitative insight into the changes of the microvasculature in infarcted and non-infarcted (remote) areas, at different time-points, following myocardial infarction. We used thick slices ($\sim 100\mu\text{m}$) of pig heart tissue, stained for blood vessels and imaged with high resolution microscope. Firstly, the cardiac microvasculature was segmented using a novel 3D multi-scale multi-thresholding approach. We subsequently calculated: i) fractal dimension to assess the complexity of the microvasculature; ii) lacunarity to assess its spatial organization; and iii) succolarity to provide an estimation of the microcirculation flow. The measures were used for statistical change analysis and classification of the distinct vascular patterns in infarcted and remote areas, demonstrating the potential of the approach to extract quantitative knowledge about infarction-related alterations.

1 Introduction

Cardiovascular diseases (CVDs) result in the alteration of microvasculature [14]. Therefore, there is increased interest in gaining deeper knowledge of the microvascular patterns and their changes during the development of CVDs in an effort to identify the underlying biological mechanisms and develop more efficient therapeutic approaches. Advances in imaging systems, particularly in high

* This research is funded by the European Commission (FP7-PEOPLE-2013-ITN ‘CardioNext’, No. 608027) and La Marató de TV3 Foundation. CNIC is supported by the MINECO and the Pro-CNIC Foundation. Kerri-Ann Norton is funded by the American Cancer Society Postdoctoral Fellowship. The authors would like to thank Jaume Agüero for performing the infarction in the pigs.

resolution microscopy, allow visualization at sub-micrometer resolution and increasing depths of the three-dimensional (3D) microvasculature [13], which is inaccessible by other imaging technologies.

However, understanding and identifying changes in the 3D structure of the microvasculature not only requires the use of state-of-the-art imaging techniques, but also the use of unbiased image analysis methods that allow the translation of qualitative biological observations into quantitative knowledge. Furthermore, automatic 3D image analysis allows extracting information not attainable from traditional manual analysis, and at the same time, diminishes subjectivity problems, time and labor requirements, of both manual and supervised analysis.

Nevertheless, even in the case of automatic analysis, the problem of identifying measures that can optimally describe highly complex structures, their changes and structural-function relations remains a challenging task. Traditional analysis provide information of paramount importance regarding vessel structure and function, but is insufficient when dealing with complex objects [7], such as biological samples, which can be self-similar, i.e. fractals. The concept of fractals was introduced by [10] and ever since they have been applied in a variety of image analysis and pattern recognition problems. In the biomedical field, they found great appeal in the study of vascular networks [9].

This paper provides a quantitative approach of describing changes that occur to the cardiac microvasculature at different time-points, after myocardial infarction (MI), at remote and infarcted regions. To achieve this, while also accommodating the complex and multi-scale properties of the microvasculature, a 3D fractal-based approach was followed. To the best of our knowledge this is the first effort made to apply a complete 3D fractal-based analysis (fractal dimension, lacunarity, succolarity) to quantitatively assess progressive MI-related changes of the microvascular patterns. In biological terms, the higher the fractal dimension, the higher the morphological complexity is, i.e. the number of microvessels. The higher the lacunarity, the more heterogeneous the gap distribution and as a result the blood supply within the tissue is. The higher the succolarity, the larger the amount of blood that can flow in the vessels, thus the better the oxygenation. Furthermore, a simple, but efficient, 3D method is proposed for the segmentation of vascular structures from images stained for blood vessels.

2 Methods

2.1 Data Acquisition and Pre-processing

All experiments were approved by the Institutional Animal Research Committee. Three adult male Large-White pigs were anesthetized and acute MI was induced using an angioplasty balloon with 30-minute occlusion of the left anterior descending coronary artery followed by reperfusion. The pigs were sacrificed 1, 3 and 7 days after reperfusion.

Tissue samples from both infarcted and remote areas from each left ventricle were collected. Samples were fixed with 0.4% paraformaldehyde, embedded in

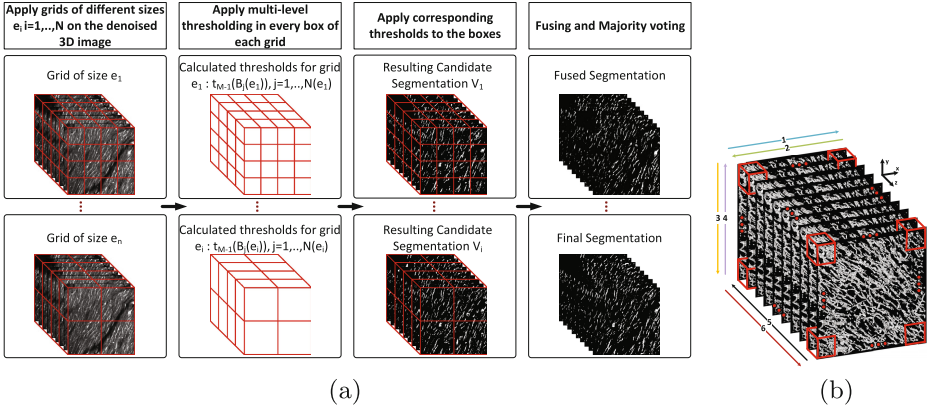


Fig. 1. (a) Overview of MMT method. (b) Possible directions of blood flow through the segmented microvasculature; horizontal flow from left to right (arrow 1) and vice versa (arrow 2), vertical flow from up to down (arrow 3) and vice versa (arrow 4), and in depth blood flow from upper to lower slices (arrow 5) and vice versa (arrow 6).

OCT and frozen down. Thick sections ($\sim 100\mu\text{m}$) were obtained in the cryostat, stained in flotation for the microvasculature with primary antibody anti-VE-Cadherin (Santa Cruz) 1:100, and incubated with secondary antibodies, Alexa-Fluor 568 (Molecular probes) 1:500 and Hoechst (Life Technologies) 1:10000.

Spectral imaging was performed with a Leica SP5 confocal microscopy using emission from a 561nm laser and $40\times/1.25\text{N.A.}$ oil immersion lens. Z-stack slices (1024×1024 pixels) were acquired every $1\mu\text{m}$ by applying the deepness correction setup. The resulting voxel size was $0.3785\mu\text{m} \times 0.3785\mu\text{m} \times 1.007\mu\text{m}$.

Prior to proceeding with the analysis, Non-Local Means Filtering [4], was adapted for enhancing the quality of the images.

2.2 Segmentation

A 3D multi-scale multi-level thresholding approach (MMT) was developed for the segmentation of the labeled vessels from confocal images, inspired by the box counting (BC) method [3] and Otsu's multi-level thresholding method [12].

Grids of varying size e were overlaid onto the image under investigation. Subsequently, the multi-level thresholding was applied to each box $B_j(e)$, $j = 1, \dots, N(e)$ of the grid with size e in order to calculate the M intensity classes that maximize the inter-class variance within the box. For every grid, $N(e)$ thresholds (t_M), as many as the boxes that composed it, were therefore calculated and applied to the corresponding box. In total, k candidate segmentations V_i , $i = 1, \dots, k$ were produced, one per grid size e , as a mosaic of the application of the $N(e)$ thresholds on the boxes. Only voxels that belong to the two classes with higher intensity ($M - 1, M$) were considered as parts of the microvasculature. Thus,

$$V_i(u) = \begin{cases} 1, & I(u) \geq t_{(M-1)}(B_j(e)) \\ 0, & I(u) < t_{(M-1)}(B_j(e)) \end{cases} \quad (1)$$

where voxel $u = (x, y, z) \in B_j(e)$ and I the original image.

Subsequently, candidate segmentations $V_i, i = 1, \dots, k$ had to be fused into a single segmentation. To achieve this, majority rule voting applied:

$$V(u) = \frac{\sum_{i=1, \dots, k} w_i V_i(u)}{\sum_{i=1, \dots, k} w_i}, \quad (2)$$

where w_i are the weights that define the degree to which candidate segmentation V_i will contribute to the final segmentation and were set to 1 considering equal contribution of all candidate segmentations.

An overview of the MMT method is presented in Fig. 1 (a). It is worth mentioning that in the traditional BC, cubic boxes compose the grid. However, here, boxes of size $e \times e \times e_z$ with $e_z = 10 < e = 2^5, \dots, N$, were used in order to accommodate for the smaller size of our images along z-direction and to cover a wide range of scales while ignoring the smaller ones that provide a very limited region for variance calculation.

2.3 Fractal-Based Methods

Fractal Dimension. A variety of methods have been proposed for the calculation of fractal dimension [8]. Among them, the box-counting method (BC), which is the most popular and widely used approach, was applied in this work. Grids of cubic boxes of size e are overlaid on the original image. Subsequently, the fractal dimension (F_d) is defined as the negative slope of the bi-logarithmic plot of the number of boxes N_e needed to cover the microvasculature as a function of the box size e . Thus,

$$F_d = - \lim_{e \rightarrow 0} \frac{\log(N_e)}{\log(e)}. \quad (3)$$

However, real-life objects might not present self-similarity over an infinite range of scales but rather over finite [9,2]. To deal with this limitation, we followed the procedure presented in [2] to identify cut-offs scales for which the microvasculature can no longer be considered as fractal. However, no statistically significant difference was observed between the calculation of fractal dimension with and without cut-offs and the former is presented in this document.

Lacunarity. The gliding box (GB) method [1] was used for the calculation of lacunarity L . According to the GB method, boxes of different sizes are glided every 1 voxel over the image and the number of voxels inside the boxes belonging to the structure of interest, i.e. voxels with value 1, are calculated and represent box mass M . Therefore, for each box size e , lacunarity is calculated by the first and second moments of inertia of mass distribution

$$L(e) = \frac{\sum_{e=1, \dots, N} M(e)P(M, e)}{\sum_{e=1, \dots, N} M(e)^2 P(M, e)}, \quad (4)$$

where $P(M, e) = \frac{n(M, e)}{N(e)}$, $n(M, e)$ stands for the number of boxes with mass M and $N(e)$ for the number of boxes of size e .

When comparing images with different densities, one limitation presented by lacunarity is its dependence on image density. To tackle this incompatibility, we used the normalized lacunarity (L_{norm}) as proposed by [5],

$$L_{norm}(e) = 2 - \left(\frac{1}{L(e)} + \frac{1}{cL(e)} \right), \quad (5)$$

where $cL(e)$ is the lacunarity the complemented image ($cL(e)$). This formulation results in lacunarity values that are in the range $[0, 1]$, allowing comparison among images with different densities. The lacunarity over all scales is defined by the mean along all scales.

Succolarity. Although succolarity (S) was firstly described by Mandelbrot [10], the first formal definition and method for its calculation, based on an adaption of BC method, was proposed recently by [11]. In brief, regions, i.e. blood vessels in the case of this study, that a fluid, i.e. blood, can flow are represented by 1 while obstacles to the fluid with 0. For the 3D case, 6 different directions that the blood can flow through the vascular structure are defined as shown in Fig. 1(b).

A segmented image V is therefore decomposed in six 3D images V_d one per direction $d = 1, \dots, 6$. Subsequently, the BC method is applied to each V_d . The number of voxels with value 1 is calculated $n(e)$, as well as the pressure (P) of the flow in each box by the coordinates of the centroid of the box, following the direction under investigation. The normalized succolarity is given by

$$S(d, e) = \frac{\sum_{e=1, \dots, N} O(e)P(e)}{\sum_{e=1, \dots, N} P(e)}, \quad (6)$$

where $O = \frac{n(e)}{e}$ stands for the occupation percentage of boxes of size e .

Ultimately, in this work, overall succolarity was approximated by its maximum value among all 6 directions, i.e. the dominant direction of blood flow.

3 Results

Fifty-four 3D confocal images, nine for each tissue category, were used for the analysis of the infarcted heart microvasculature. For simplicity, images corresponding to tissue from infarcted and remote areas, 1 day, 3 and 7 days post MI were abbreviated as I1MI, R1MI, I3MI, R3MI, I7MI, and R7MI.

Firstly, the outcome of the multi-scale multi-thresholding method was visually evaluated by an experienced biologist in order to avoid bias in the analysis due to erroneously segmented images. In solely one case out of fifty-five the segmentation outcome was considered unsatisfactory.

In order to quantify alterations in the complexity, gap distribution and/or microcirculation of the microvasculature, as expressed quantitatively by fractal dimension, lacunarity and succolarity, statistical change analysis was performed. To achieve this, we applied Wilcoxon rank sum tests and Multi-variate analysis of variances (MANOVA) to perform pairwise comparisons of the characteristics

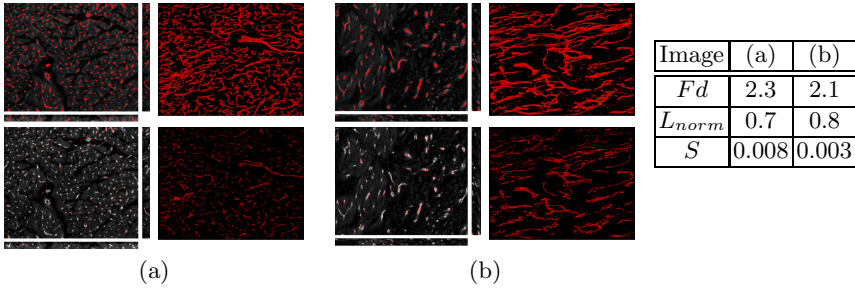


Fig. 2. Example segmentations by means of MMT method (first row) and of traditional multi-level thresholding (second row) from remote (a) and from infarcted area (b) along with the corresponding 3D fractal measures. The segmented vessels are presented with red on the slices along x-y,y-z,x-z (right) and on the 3D reconstructions (left).

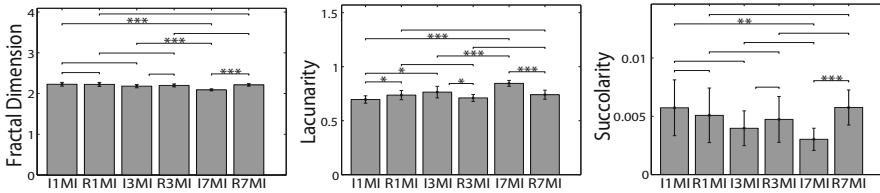


Fig. 3. Statistical comparison by means of (i) Fractal Dimension, (ii) Lacunarity, (iii) Succularity, where *, ** and *** represent p-value < 0.05, 0.01 and 0.001 respectively.

Table 1. Multivariate Anova. P-values for cases that the null hypotheses is rejected at the 1 % significance level are shown in bold.

I1MI - R1MI	$p = 0.0039$	I1MI - I3MI	$p = 0.056$	R1MI - R3MI	$p = 0.0122$
I3MI - R3MI	$p = 0.0702$	I1MI - I7MI	$p < 10^{-9}$	R1MI - R7MI	$p = 0.0367$
I7MI - R7MI	$p = 10^{-6}$	I3MI - I7MI	$p < 10^{-7}$	R3MI - R7MI	$p = 0.2383$

Table 2. Accuracy (%) in classifying the distinct vascular patterns using different classifiers: (1) Knn, (2) SVM, (3) Adaboost.

Classifier	1	2	3	Classifier	1	2	3	Classifier	1	2	3
I1MI - R1MI	58	73	75	I1MI - I3MI	58	75	83	R1MI - R3MI	68	73	79
I3MI - R3MI	64	71	57	I1MI - I7MI	100	100	100	R1MI - R7MI	52	57	72
I7MI - R7MI	100	100	100	I3MI - I7MI	79	100	86	R3MI - R7MI	53	60	65

of the microvasculature from infarcted vs remote areas at all time-points, and of the same tissue area progressively in time.

Fig. 2 provides examples of the performances of MMT method and traditional multi-level thresholding on two images of our dataset, along with the calculated metrics for comparison purposes.

Table 1 provides the p-values for all pairwise comparisons performed by means of MANOVA. The null hypothesis, that there is no statistically significant differences between the infarct and remote areas, was rejected in the case of I1MI vs R1MI and in that of I7MI vs R7MI. This implies significant differences regarding the space filling properties of the microvessels (fractal dimension, lacunarity) and microcirculation. Of particular interest is the fact that 3 days after MI the null hypothesis is not rejected. This, in conjunction with recent work by [6] on the bimodal pattern of edema after MI, makes the study of changes at 3 days post MI a point for further investigation. I1MI and I3MI differ significantly from I7MI, but not among them, while remote areas at different time-points present no significant differences.

Fig. 3 presents plots which indicate mean values, standard deviations and p-values, resulting from Wilcoxon rank sum tests, for the statistical change comparison in terms of each fractal measure independently. A statistically significant decreased complexity, expressed by fractal dimension, was observed between I1MI and I3MI, when compared with I7MI. In contrast, a progressively increased varying distribution of gaps was observed by means of lacunarity. This inversely proportional relation between fractal dimension and lacunarity might be related to a wider range of sizes of microvessels. In fact, 7 days post MI apart from capillaries, larger vessels were observed, as also reported in the canine MI model [15]. Moreover, by comparing succolarity in infarcted areas 1 and 7 days post MI, functional changes related with microcirculation were added to the structural, expressed by fractal dimension and lacunarity. As it might have been expected, there was no measure that presented significant differences for remote areas at progressing time-points. As far as between infarcted and remote areas comparisons are concerned, gap distribution, presented statistically significant differences at all time-points under comparison, which makes lacunarity the most sensitive among the measures compared. Differences between remote and infarcted areas became clear in terms of all metrics only 7 days post MI.

Ultimately, we incorporated the metrics into a classification scheme. The classifiers used are, (i) K-nearest neighbor classifier (knn), (ii) Support Vector Machines (SVM), and (iii) Adaboost [17]. In all cases, 9-fold cross validation repeated 100 times was used. Accuracy rates (%) are presented in Table 2. The classifiers demonstrated similar behavior with higher accuracy in those pairs of comparisons for which MANOVA had demonstrated differences. In addition, Adaboost and SVM classifiers achieved more than 70 and 75 % accuracy respectively, for all of those cases. This demonstrates the power of fractal measures to describe and identify between different microvascular patterns post infarction.

4 Conclusions

We proposed the use of a 3D fractal-based approach to quantify infarction-related changes of the microvasculature at three different time-points after MI. 3D confocal images stained for blood vessels of both infarcted and remote areas were used. The animal model chosen was the pig due to its high translational

value related with the similarity of its coronary artery anatomy and distribution to those of humans [16].

Statistically significant changes in terms of structure (fractal dimension and lacunarity) and function (succolarity) were detected by means of significance tests and MANOVA. Furthermore, relatively high rates of correct classification of unseen 3D microvascular images into distinct tissue categories, based on just their complexity, gap distribution and dominant blood flow as expressed by the applied fractal measures, demonstrate their potential to describe and recognize characteristics and changes due to infarction at the microvascular level.

References

1. Allain, C., Cloitre, M.: Characterising the lacunarity of random and deterministic fractal sets. *Phys. Rev. Lett.* 44, 3552–3558 (1991)
2. Berntson, G.M., Stoll, P.: Correcting for Finite Spatial Scales of Self-Similarity When Calculating Fractal Dimensions of Real-World Structures. *Proceedings of the Royal Society B: Biological Sciences* 264(1387), 1531–1537 (1997)
3. Block, A., von Bloh, W., Schellnhuber, H.J.: Efficient box-counting determination of generalized Fractal Dimensions. *Physical Review A* 42, 1869–1874 (1990)
4. Buades, A., Coll, B., Morel, J.-M.: A non-local algorithm for image denoising. In: *CVPR* (2), pp. 60–65 (2005)
5. Dougherty, G., Henebry, G.M.: Fractal signature and lacunarity in the measurement of the texture of trabecular bone in clinical CT images. *Med. Eng. Phys.* 23(6), 369–380 (2001)
6. Fernández-Jiménez, R., Sánchez-González, J., Agüero, J., et al.: Myocardial Edema After Ischemia/Reperfusion Is Not Stable and Follows a Bimodal Pattern: Imaging and Histological Tissue Characterization. *J. Am. Coll. Cardiol.* 65(4), 315–323 (2015)
7. Gould, D.J., Vadakkan, T.J., Poché, R.A., Dickinson, M.E.: Multifractal and Lacunarity Analysis of Microvascular Morphology and Remodeling. *Microcirculation* 18(2), 136–151 (2011)
8. Lopes, R., Betrouni, N.: Fractal and multifractal analysis: a review. *Med. Image Anal.* 13(4), 634–649 (2009)
9. Lorthois, S., Cassot, F.: Fractal analysis of vascular networks: insights from morphogenesis. *J. Theor. Biol.* 262(4), 614–633 (2010)
10. Mandelbrot, B.B.: *Fractal geometry of nature*. Freeman, New York (1977)
11. Melo, R.H.C., Conci, A.: How Succolarity could be used as another fractal measure in image analysis. *Telecommunication Systems* 52(3), 1643–1655 (2013)
12. Otsu, N.: A Threshold Selection Method from Gray-Level Histograms. *IEEE Transactions on Systems, Man, and Cybernetics* 9(1), 62–66 (1979)
13. Pawley, J.B.: *Handbook of Biological Confocal Microscopy*. Springer (2006)
14. Petersen, J.W., Pepine, C.J.: Microvascular coronary dysfunction and ischemic heart disease: Where are we in 2014? *Trends Cardiovasc. Med.* 25(2), 98–103 (2015)
15. Ren, G., Michael, L.H., Entman, M.L., Frangogiannis, N.G.: Morphological characteristics of the microvasculature in healing myocardial infarcts. *J. Histochem. Cytochem.* 50(1), 71–79 (2002)
16. Weaver, M.E., Pantely, G.A., Bristow, J.D., Ladley, H.D.: A quantitative study of the anatomy and distribution of coronary arteries in swine in comparison with other animals and man. *Cardiovasc. Res.* 20(12), 907–917 (1986)
17. Wu, X., Kumar, V., Quinlan, J.R., et al.: Top 10 algorithms in data mining. *Knowledge and Information Systems* 14(1), 1–37 (2008)